

---

# Earthquake Cycles on the San Andreas Fault System in Northern California

M. Burak Yıkılmaz, Don L. Turcotte, Olga Beketova, Louise H. Kellogg, and John B. Rundle

---

## Abstract

The 24 August, 2014,  $M=6.0$  South Napa earthquake was the first earthquake to significantly affect the populous San Francisco Bay region since the 1989 Loma Prieta earthquake. The Napa earthquake has resulted in a new interest in earthquake risk on the San Andreas Fault (SAF) system north of San Francisco. The deformation in this region is dominantly right lateral shear between the rigid Pacific Plate and the rigid Sierra-Nevada-Central-Valley Plate. GPS observations are well approximated by a uniform shear strain across this 100 km wide zone. This zone is recognized to be a “slab window” with a relatively thin lithosphere. In this paper, we hypothesize that this lithosphere is composed of a 12 km thick brittle elastic upper lithosphere and a 15 km thick viscoplastic lower lithosphere. We attribute the observed near uniform surface strain to flow in the viscoplastic zone. Deformation in the brittle upper lithosphere results in seismicity. A substantial fraction, about  $20 \text{ mm year}^{-1}$ , of the  $32 \text{ mm year}^{-1}$  of the right lateral deformation takes place on the SAF. However, the SAF is not parallel to the motion of the bounding rigid plates. This geometrical incompatibility requires distributed deformation across the 100 km wide zone. A fraction of this distributed deformation takes place on three relatively well defined strike-slip fault zones to the east of the SAF as well as on other faults. We suggest that when a large earthquake occurs, the localized stress concentrations are relaxed by flow in the viscoplastic zone. We give a detailed description of this process during and following the 1906 earthquake and show the process is consistent with observations. We also relate our tectonic model to the present distribution of seismicity in our study area.

---

## Keywords

Earthquakes • GPS • Northern California • Tectonics • Uniform shear

---

## 1 Introduction

The San Andreas Fault (SAF) is a primary boundary between the Pacific Plate (PP) and the North American Plate (NAP). However, the associated deformation occurs over much of the

western United States. In this paper, we focus our attention on the SAF system in northern California. We consider this region for several reasons. The geometry is relatively simple since the zone of deformation is bounded on the west by the near rigid PP and on the east by the near rigid Sierra-Nevada Central-Valley Plate (SNCVP) (Fig. 1a). The deformation in this zone is transpression with some  $32 \text{ mm year}^{-1}$  of right lateral strike-slip displacement and about  $3 \text{ mm year}^{-1}$  of compression. There are many strike-slip faults in the zone with parallel ranges that absorb the compressional component. The strike-slip displacement is primarily accommodated on the SAF with  $16\text{--}27 \text{ mm year}^{-1}$  displacement.

---

M.B. Yıkılmaz (✉) • D.L. Turcotte • O. Beketova • L.H. Kellogg • J.B. Rundle  
Department of Earth & Planetary Sciences, University of California Davis, One Shields Ave, Davis, CA 95616, USA  
e-mail: [mbyikilmaz@ucdavis.edu](mailto:mbyikilmaz@ucdavis.edu); [dlturcotte@ucdavis.edu](mailto:dlturcotte@ucdavis.edu); [obeketova@ucdavis.edu](mailto:obeketova@ucdavis.edu); [kellogg@ucdavis.edu](mailto:kellogg@ucdavis.edu); [jbrundle@ucdavis.edu](mailto:jbrundle@ucdavis.edu)

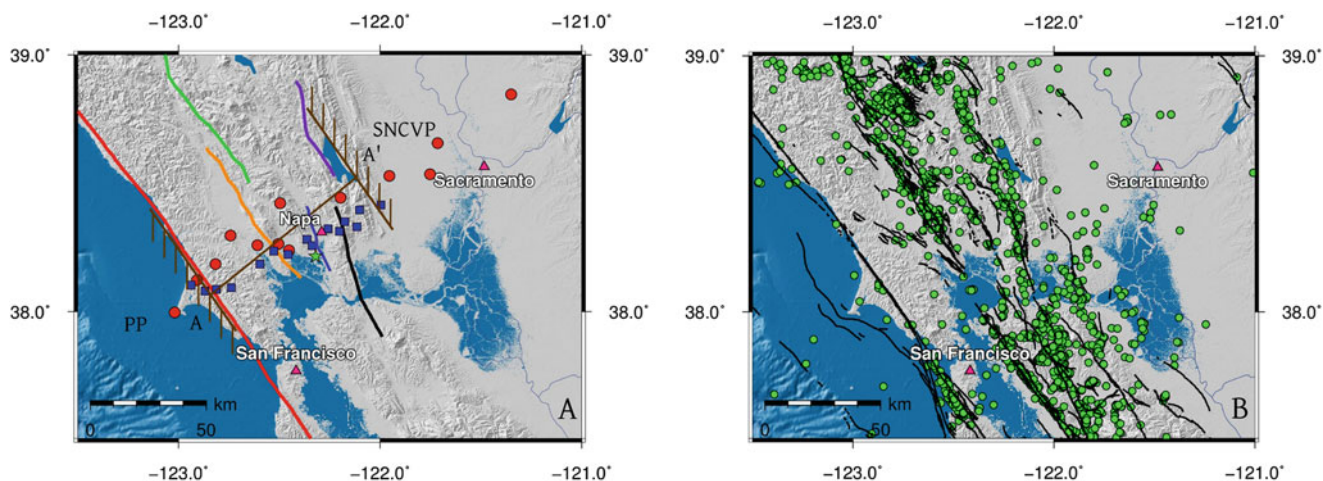


**Fig. 1** (a) Illustration of the transect A-A' upon which we base our study of the seismic cycles on the San Andreas fault system. The 100 km wide zone of deformation is bounded by the rigid Pacific Plate (PP) and the rigid Sierra Nevada Central Valley Plate (SNCVP). The major faults in the zone of deformation are shown: San Andreas (red), Maacama (green), Rodgers Creek (orange), West Napa (blue), Bartlett Springs

(purple), and Green Valley (black). Also shown are continuous GPS stations (red circles) and campaign GPS stations (blue squares). Green star along the West Napa fault indicates the epicenter of the August 24, 2014 earthquake. (b) Distribution of  $M > 2$  earthquakes in the study region during the period 2000–2010

Strike-slip deformation is also attributed to three sub-parallel fault systems to the east of the San Andreas (Freymueller et al. 1999; D'Alessio et al. 2005). The first of these is the Rodgers Creek Fault (RCF). This is a well-defined fault with an  $6\text{--}11\text{ mm year}^{-1}$  displacement. The RCF is the northern extension of the Hayward fault to the south. Further to the east, strike-slip deformation is documented on the West Napa (WNF) and the Concord-Green Valley (CGVF) faults. These are not well defined geologically and the displacements are poorly known. These faults are suggested to be the northern extension of the Calaveras Fault to the South. The last great earthquake in the study region was the 18 April, 1906 San Francisco earthquake on the SAF. Felt intensity studies indicated that this earthquake had a magnitude of about  $M = 8.0$ . Displacements averaging about 4 m extended over some 200 km including our study region. Triangulation data are available to assess both the coseismic deformation and the subsequent stress relaxation process (Thatcher 1974, 1975; Matthews and Segall 1993). The first moderate earthquake to occur in our study region since the 1906 earthquake was the 24 August, 2014,  $M = 6.0$  South Napa earthquake. This earthquake occurred on a branch of the West Napa fault and had right-lateral, strike-slip surface deformation extending over some 15 km with a maximum offset of about 460 mm.

Strain rates across our zone of deformation are obtained using GPS data. We utilize observations obtained on the transect A-A' across the zone of deformation as illustrated in Fig. 1a. This transect is chosen because of the availability of relevant data in the region. Specifically the use of strain data associated with the 1906 coseismic deformation and

subsequent strain relaxation as well as the current GPS strain field. This transect also includes the rupture of the 2014 South Napa earthquake.

The measured velocities at the stations shown in Fig. 1a are given in Fig. 2. These velocities are parallel to the trend of the SAF and are relative to the stable NAP. Included are both continuous GPS observations from the beginning of the records in the 2000s up to 1 January 2011 and campaign GPS observations during various intervals during the 1990s. We interpret this observed behavior to reflect a region of near uniform shear strain between the rigid PP and the rigid SNCVP. This region is a 100 km wide zone extending across the Coast Ranges from 20 km west of the SAF to 80 km east of the SAF. Based on the linear correlation given in Fig. 2, we take the velocity across the 100 km wide deformation zone to be  $32\text{ mm year}^{-1}$  and the uniform shear strain to be  $\dot{\epsilon} = 0.32\ \mu\text{strain year}^{-1}$ . A number of authors have previously recognized the near linear strain field given by the GPS data (D'Alessio et al. 2005; Freymueller et al. 1999; Prescott et al. 2001; Smith and Sandwell 2003; Johnson and Segall 2004; Savage et al. 2004; Jolivet et al. 2009). Several of these authors have utilized block models for the earthquake cycle on independent faults to explain the strain field in this region. Various block models and a wide range of parameter values have been used by these authors. For comparison with the linear strain field in Fig. 2, we derive a strain field expected for a block model. We consider a block model that extends a uniform vertical strike-slip fault to infinite depth. Beneath a locking depth  $d$ , a uniform slip velocity  $V_a$  is applied across the fault. The earthquake rupture occurs above the locking depth. The surface velocity distribution  $V_s(x)$  during strain

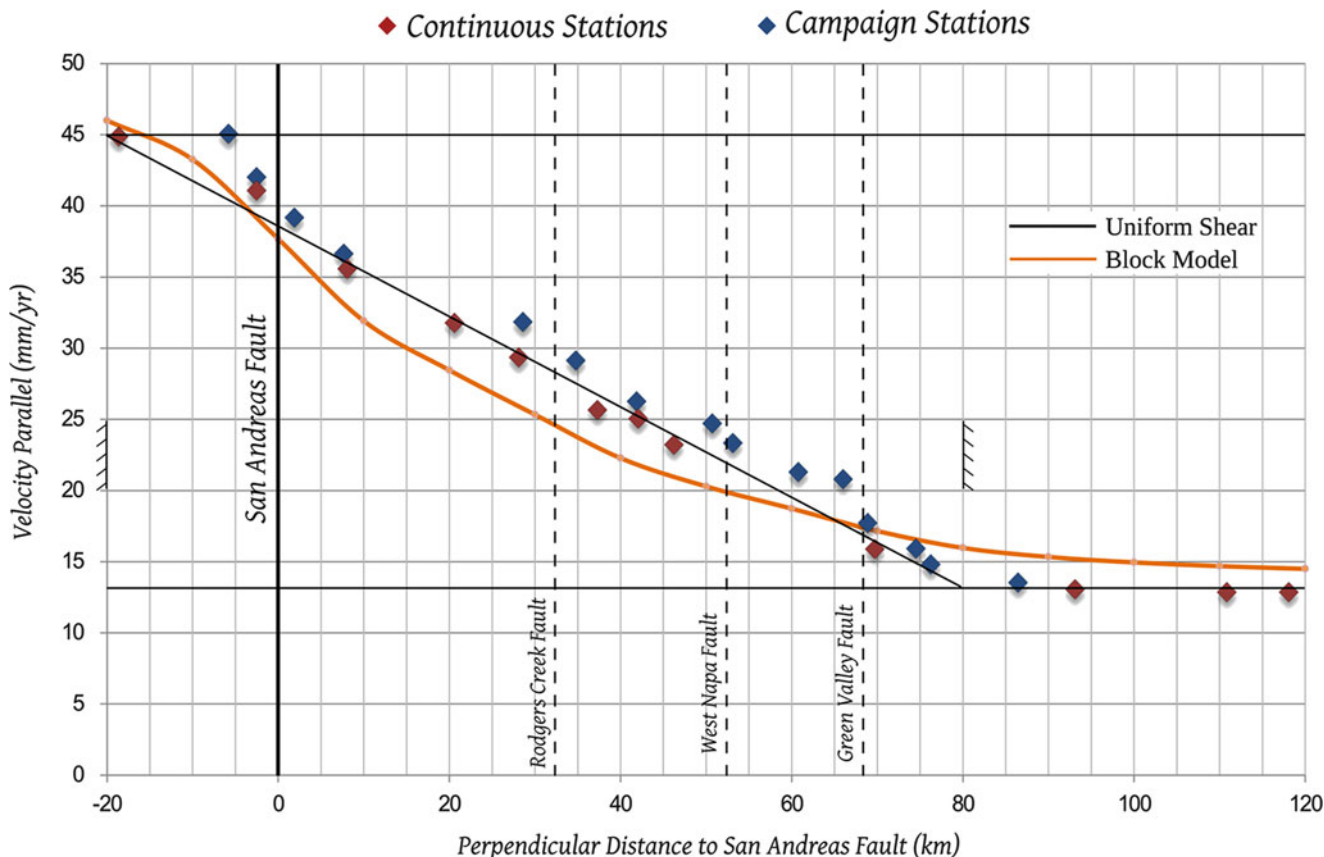


**Fig. 2** Velocities of the GPS stations illustrated in Fig. 1. These velocities are relative to the stable North American Plate. We give the velocity components parallel to the SAF as a function of the distance from the

SAF. Also shown is the linear correlation with the data that we use in this paper and the velocity distribution for our block model from Eq. (1)

accumulation is given by Freymueller et al. (1999):

$$V_s = V_a \left( \frac{1}{2} + \frac{1}{\pi} \tan^{-1} \left( \frac{x - x_f}{d} \right) \right) \quad (1)$$

where  $x_f$  is the location of the fault and  $x - x_f$  is the distance normal to the fault. The surface velocity distribution depends on the prescribed slip velocity  $V_a$  and the locking depth  $d$ . The solution given in Eq. (1) is for an elastic half-space with uniform properties but does not depend on the elastic rigidity.

For our block model we consider four parallel strike-slip faults separated by three internal blocks with two boundary blocks. The partitioning of slip between these four faults depends on geological data. Detailed studies of this distribution of slip have been obtained recently in order to constrain the Uniform California Earthquake Rupture Forecast, version 3 (UCERF3). Estimated slip rates with bounds for the four faults that we study have been given by Dawson and Weldon (2013). These are, with their comments;

1. San Andreas (North Coast). Best estimate: 24 mm year<sup>-1</sup>, bounds (16–27 mm year<sup>-1</sup>). UCERF3 slip rate based on reported geologic rates.

2. Rodgers Creek. Best estimate: 9 mm year<sup>-1</sup>, bounds (6–11 mm year<sup>-1</sup>). UCERF3 slip rate based on reported geologic rate and rate on Hayward Fault. Note that slip rate is tapered in the area of overlap with the Maacama Fault so that the rate along this system is not doubly counted.
3. West Napa. Best estimate: 1 mm year<sup>-1</sup>, bounds (1–5 mm year<sup>-1</sup>). UCERF3 adopts the UCERF2 assigned rate because there is no direct slip rate available. Slip rate bounds expanded based on mapping by Clahan (2011) that suggests fault may be more active than previously thought.
4. Green Valley. Best estimate: 4 mm year<sup>-1</sup>, bounds (2–9 mm year<sup>-1</sup>). Rate based on reported geologic rate and USGS category, as well as the rate on the adjacent Concord Fault. Upper bound assigned based on upper bound on Concord Fault.

Assuming all deformation across the deformation zone occurs on the four faults (required by the block model), the total slip given by UCERF3 is 38 mm year<sup>-1</sup>. This compares with our preferred value of 32 mm year<sup>-1</sup> from the GPS data given in Fig. 2.

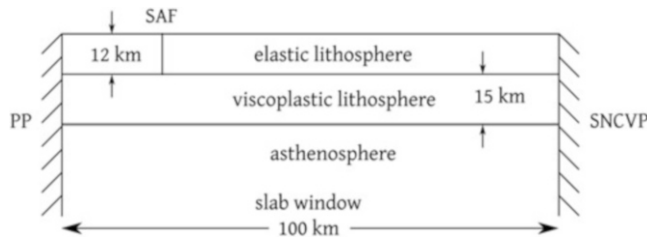


**Fig. 3** Illustration of our model for the behavior of deformation in the slab window between the rigid PP and the rigid SNCVP (transect A-A' in Fig. 1)

In addition to the preferred slip velocities given above, we take the locking depth of each fault to be  $d = 12$  km. This is typical of values selected by previous authors (i.e. Smith and Sandwell 2003) and is consistent with the maximum depth of seismicity. The San Andreas Fault is at  $x_f = 0$  km, the Rodgers Creek Fault at  $x_f = 32$  km, the West Napa Fault at  $x_f = 52$  km, and the Green Valley fault at  $x_f = 68$  km. The velocity field across the zone of deformation is obtained by solving Eq. (1) for each of the four faults and adding the results (appropriate for linear elasticity).

The velocity distribution obtained by our block model is given in Fig. 2. There are clearly significant difference between the block model results and the observed linear strain field. The primary cause for this difference is the dominant role played by the San Andreas Fault. A slip velocity of  $24 \text{ mm year}^{-1}$  out of a total slip of  $38 \text{ mm year}^{-1}$  (63% of the total). The San Andreas velocity field dominates the total strain field causing a significant deviation from the linear observed behavior. In order for the block model to be consistent with the observed near uniform strain, a significant reduction of the slip velocity on the San Andreas Fault would be required. Considering the uncertainties this is possible, but we consider it to be highly unlikely.

The block model described above implies that the strain accumulation and release cycles on the three major faults are only weakly coupled. The observed uniform strain field requires equal partitioning of stress accumulation to the three faults. The purpose of this paper is to propose a model for the region that explains the partitioning of coseismic slip on the three faults with uniform strain accumulation. Chéry (2008) also argued against the block model and concluded that the uniformity of the shear strain is evidence that the 100 km wide region between the two rigid plates is relatively soft.

## 2 Proposed Model

This paper utilizes the model illustrated in Fig. 3. We postulate a 12 km thick elastic lithosphere based on the depth of earthquakes in the deformation zone. In this brittle elastic lithosphere, deformation is dominated by displacements on

faults. We further postulate a 15 km thick viscoplastic lower lithosphere (lower crust). The near-uniform deformation in this zone results in the near-uniform shear strain illustrated in Fig. 2. Beneath the lithosphere, the mantle asthenosphere is sufficiently weak to provide little resistance to the shearing motion. The thin brittle lithosphere responds to the near uniform shear deformation imposed by the bounding rigid plates and the near uniform shear strain in the viscoplastic lower lithosphere. Because of the geometrical incompatibility between the orientation of the SAF and the imposed deformation at the rigid plate boundaries, the brittle lithosphere is subjected to distributed internal deformation. Some of the deformation occurs on the three faults described above. When an earthquake occurs, like the 2014 South Napa earthquake, the localized coseismic deformation is redistributed by viscoplastic deformation of the lower crust.

The thin lithosphere and the deformable region beneath are attributed to the recent subduction of the Farallon Plate (FP) beneath the SNCVP in northern California. The separation of the FP from the PP left a gap in the lithosphere. This gap, known as a slab window, extends from the PP to the SNCVP as illustrated in Fig. 1. The GPS data given in Fig. 2 clearly illustrate the boundaries of the slab window and the near uniform strain accumulation to the West. The eastern boundary is at 80 km from the San Andreas Fault as shown. The SNCVP is basically rigid, implying a thick lithosphere. The eastern boundary is at the San Andreas Fault. Strain accumulation associated with earthquakes on the San Andreas Fault is predominantly to the east in the thinner lithosphere. Furlong and Schwartz (2004) have presented details of the slab window hypothesis.

The slab window is characterized by high heat flow and volcanism. Lachenbruch and Sass (1980) demonstrated high heat flow in the slab window region. The thin lithosphere hypothesis is further solidified by studies of the extensive recent volcanism throughout the slab window region (Dickinson 1997). Our objective is to present a model for the earthquake cycle in the study region. Our study of the earthquake cycle begins with the coseismic behavior associated with the 1906 San Francisco earthquake. Thatcher (1974, 1975) and Matthews and Segall (1993) used surface and geodetic triangulation data to quantify the surface rupture during the 1906 earthquake. Based on this work we take the coseismic surface displacement to be  $\Delta w_{cs} = 4$  m and the depth of rupture to be 12 km. Consistent with these values and also with global compilations of stress drop in major earthquakes (Kanamori and Anderson 1975) we take the mean stress drop in the 1906 earthquake to be  $\Delta\sigma_{cs} = 5$  MPa. These values are illustrated in Fig. 4.

We assume the shear stress across the 100 km wide window had increased to a uniform value  $\Delta\sigma = 5$  MPa just prior to the 1906 earthquake. This assumption is based on the uniform increase in shear strain illustrated in Fig. 2 and

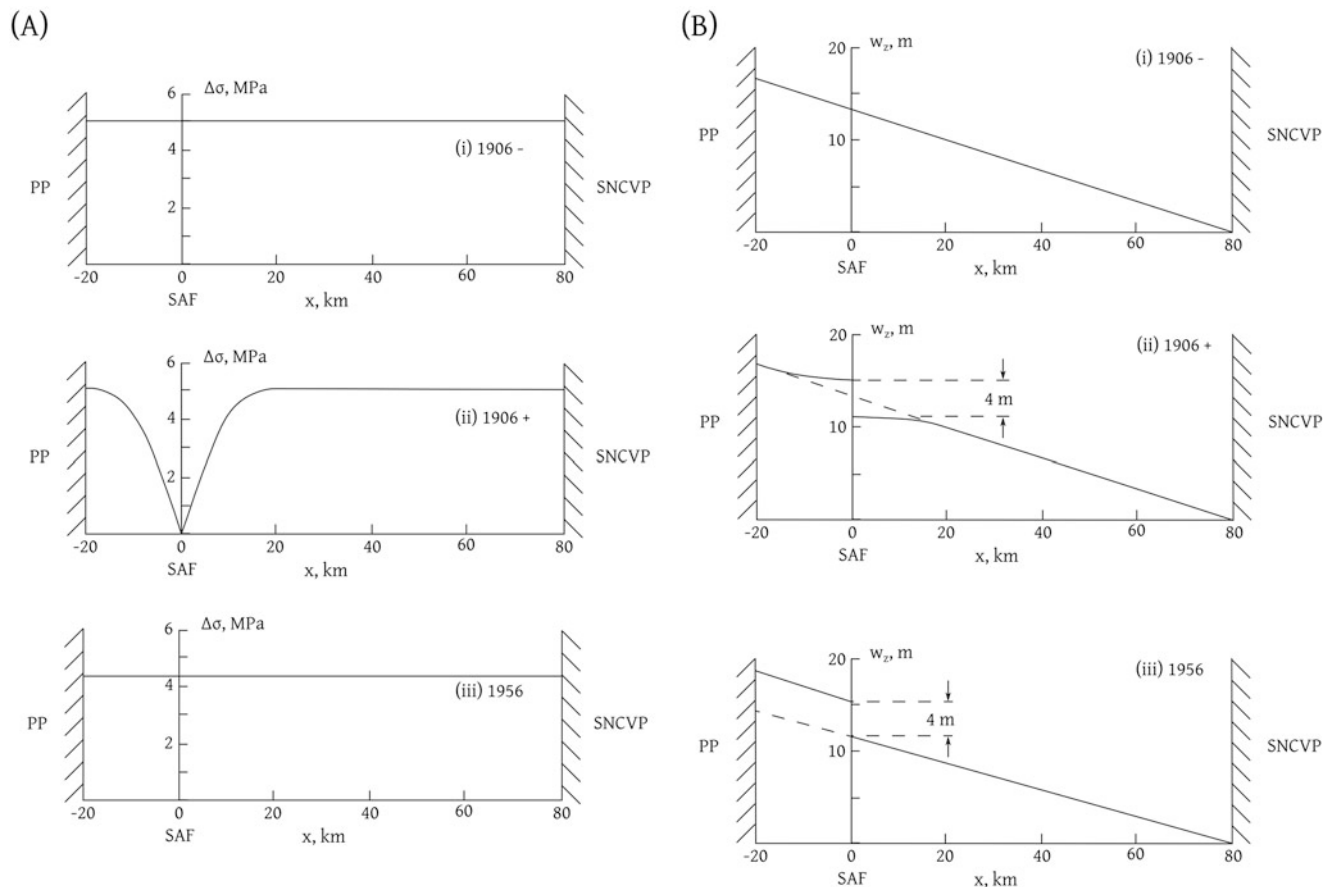


**Fig. 4** An overview of our proposed earthquake cycle on the SAF system in Northern California. In (a), we show the dependence of the excess stress  $\Delta\sigma$  during the cycle on the distance across the slab window  $x$  from the bounding PP on the southwest to the bounding SNCVP on the north east. In (b), we show the dependence of the surface

displacement  $w$  during the cycle on the distance across the slab window  $x$ . The PP is moving at a constant velocity  $32 \text{ mm year}^{-1}$  relative to the fixed SNCVP. The distribution of excess stress  $\Delta\sigma$  and displacement  $w$  are given; (i) just before the 1906 earthquake, (ii) just after the 1906 earthquake, and (iii) in 1956 after post seismic relaxation

shown in Fig. 4a(i). The total shear stress  $\sigma$  would require the addition of a uniform background stress, which is not important for our analysis since we consider only the stress (and strain) variability during an earthquake cycle. Taking  $\Delta\sigma = 5 \text{ MPa}$  and the shear modulus  $G = 30 \text{ GPa}$ , the corresponding constant shear strain  $\Delta\epsilon = \Delta\sigma / G = 1.67 \cdot 10^{-4}$ . This constant shear strain implies a linear increase in surface displacement  $w$  across the slab window. The total surface displacement is  $w = 16.7 \text{ m}$  as illustrated in Fig. 4b(i). During the earthquake the mean stress on the fault drops from  $\Delta\sigma = 5 \text{ MPa}$  to  $\Delta\sigma = 0 \text{ MPa}$  [see Fig. 4a(ii)]. Geodetic studies before and after the earthquake restrict the depth of rupture to about 12 km (Thatcher 1974, 1975; Matthews and Segall 1993). Studies of the distribution of surface stress associated with a strike-slip fault rupture have been given by Turcotte and Schubert (2014). The region that has a significantly lower stress immediately after the earthquake and its aftershocks sequence has a width of about 30 km as illustrated in Fig. 4a(ii). After the earthquake there is a large variation of the stress in the lithosphere across

the slab window (5 MPa). Because the upper lithosphere is thin, it is expected that flow in the viscoplastic lower lithosphere will lead to a relaxation of this stress difference (Yu et al. 1996; Pollitz et al. 2004, 2008; Pollitz and Nyst 2005; Pollitz and Schwartz 2008). Kenner and Segall (2000, 2003) studied the postseismic deformation following the 1906 earthquake. They utilized triangulation data from the Point Arenas and Point Reyes – Petaluma areas. They inferred that the effective relaxation time for this long-term postseismic deformation was  $36 \pm 16$  years. They also noted that deep afterslip models on a vertical fault could not explain the concentration of this deformation on the northeast side of the SAF. This concentration of the post-seismic deformation to the northeast of the SAF is consistent with stress relaxation across the 100 km wide slab window. Based on the relaxation time given above, we assume that the stress relaxation was completed by 1956. This stress relaxation leads to a reloading of the shear stress on the SAF and a reduction in the shear stress elsewhere. This state of stress and strain is illustrated in Fig. 4a(iii), b(iii).

Since 1956 we assume a steady rate of uniform shear loading associated with the deformation given in Fig. 2. The current observation of near constant shear strain has important implications for the force balance and rigidity of the lithosphere in our study region. (1) The force transmitted through the lithosphere across the region is nearly constant. (2) The rigidity of the lithosphere in the study region is also nearly constant. If this were not the case, shear strain would be variable across the region, not consistent with observations. We attribute this rigidity to the viscoplastic flow in the lower lithosphere (lower crust). The associated deformation of the brittle, elastic upper lithosphere generates earthquakes on a wide range of scales including the 2014 South Napa Earthquake.

To summarize our model based on the profiles given in Fig. 4 we have made the following assumptions:

1. The stress and strain in Fig. 4a(i), b(i) are based on the uniform distribution of strain increase inferred from the GPS observations in Fig. 2.
2. The stress and strain in Fig. 4a(ii), b(ii) are based on an analytic solution for the change in stress and strain from the prescribed 1906 rupture.
3. The stress and strain in Fig. 4a(iii), b(iii) are based on an assumption of the relaxation of stress differences across the slab window by 1956.

### 3 Seismicity

We next consider the implications of the seismicity in our study region. In Fig. 1b we show that the distribution of  $M > 2$  earthquakes in the study region during the period 2000–2010. This interval was chosen to correspond to the period during which the continuous GPS data were obtained. We also show the epicenter of the 2014 South Napa earthquake. This is the first moderate sized earthquake in the region since 1906. It is clear from the data in Fig. 1b that seismic activity is concentrated on and east of the Maacama-Rodgers Creek fault system with another concentration on the Bartlett Springs-Green Valley fault system. There is distributed seismicity between these two fault zones which including some activity on the West Napa fault system where the 2014 South Napa earthquake occurred.

The current seismicity is clearly concentrated in the eastern half of the deformation zone. We suggest that this is a consequence of the stress relaxation diffusing eastward from the western half of the zone following the 1906 earthquake. Combined with the coseismic stress

reduction, this led to a net stress increase in the eastern half of the zone causing the increase in seismicity we see today.

### 4 Discussion

Geodetic observations and seismicity demonstrate conclusively that the PP and the SNCVP plate act as rigid plates bounding the zone of deformation associated with the San Andreas Fault in our study area. The deformation zone is transpressional with some  $32 \text{ mm year}^{-1}$  of right lateral strike-slip motion and some  $3 \text{ mm year}^{-1}$  of compressional motion. These values are quite well defined by GPS observations as we have shown. A substantial fraction of the strike-slip motion is taken up on the SAF. However, the preferred value of  $24 \text{ mm year}^{-1}$  on this fault has a large uncertainty,  $16\text{--}27 \text{ mm year}^{-1}$ , because the partition of displacements between the San Andreas Fault and the rest of the zone of deformation is not well constrained.

We have shown that the GPS observations across the deformation zone are well approximated by a uniform shear strain. We argue that this uniform shear strain is evidence that the lithosphere in this zone is thin. We propose a model in which this lithosphere has thickness of about 27 km compared with 50–100 km in the bounding rigid plates. We divide this lithosphere in an upper elastic lithosphere with a thickness of 12 km (the seismogenic zone) and lower viscoplastic lithosphere with a thickness of 15 km. The shear deformation in this viscoplastic zone gives the near uniform surface shear illustrated in Fig. 2. The thickness of the lithosphere approximates the thickness of the continental crust in the deformation zone. The mantle is a low viscosity asthenosphere which responds passively to the shear motion in the lithosphere. We have attributed the thin lithosphere to the slab-window hypothesis (Furlong and Schwartz 2004). These authors have presented extensive evidence for an anomalously thin lithosphere in our study region.

At the present time the brittle-elastic upper lithosphere also responds passively to the shear deformation with a near uniform increase in the shear stress. We suggest that this increase in shear stress triggers the background seismicity illustrated in Fig. 1b. We further suggest that this increase in shear stress also triggered the 2014 South Napa earthquake. Based on observations associated with the 1906 earthquake on the SAF, the subsequent stress relaxation, and the present uniform shear we hypothesize the following earthquake cycle for this region: (1) A large earthquake occurs on one of

the major faults. The depth of rupture is about 12 km and the width of stress drop is about 30 km. (2) Stress relaxation occurs across the slab window. The stress in the lower lithosphere equilibrates, thereby reloading the fault that ruptured. (3) Uniform shear loading (as shown in Fig. 2) continues until there is again a large earthquake on one of the major faults.

**Acknowledgements** The GPS and the seismic data were obtained from UNAVCO and Advanced National Seismic System respectively.

## References

- Advanced National Seismic System (ANSS) (2012). <http://www.ncedc.org/anss/catalog-search.html>. Accessed 25 Aug 2012
- Chéry J (2008) Geodetic strain across the San Andreas fault reflects elastic plate thickness variations (rather than fault slip rate). *Earth Planet Sci Lett* 269(3–4):351–364. doi:10.1016/j.epsl.2008.01.046
- Clahan KB (2011) Paleoseismicity chronology along the Northern West Napa fault zone, Napa County, CA: U.S. Geological Survey Final Technical Report, Award Number 07HQGR0081, 6p
- D'Alessio MA, Johanson IA, Bürgmann R, Schmidt DA, Murray MH (2005) Slicing up the San Francisco Bay area: block kinematics and fault slip rates from GPS-derived surface velocities. *J Geophys Res* 110(B6):B06403. doi:10.1029/2004JB003496
- Dawson TE, Weldon RJ (2013) Uniform California earthquake rupture forecast, Version 3 (UCERF3) - The time-independent model, Appendix B, Geological slip rate data and geologic deformation model. USGS Open-File Report 2013-1165
- Dickinson WR (1997) Tectonic implications of Cenozoic volcanism in coastal California. *Geol Soc Am Bull* 109(8):936–954. doi:10.1130/0016-7606(1997)109<0936:OTIOC>2.3.CO;2
- Frey Mueller JT, Murray MH, Segall P, Castillo D (1999) Kinematics of the Pacific North America plate boundary zone, northern California. *J Geophys Res* 104(B4):7419–7441. doi:10.1029/1998JB900118
- Furlong KP, Schwartz SY (2004) Influence of the Mendocino triple junction on the tectonics of coastal California. *Annu Rev Earth Planet Sci* 32:403–433. doi:10.1146/annurev.earth.32.101802.120252
- Johnson KM, Segall P (2004) Viscoelastic earthquake cycle models with deep stress-driven creep along the San Andreas fault system. *J Geophys Res* 109(B10):B10403. doi:10.1029/2004JB003096
- Jolivet R, Bürgmann R, Houlié N (2009) Geodetic exploration of the elastic properties across and within the northern San Andreas fault zone. *Earth Planet Sci Lett* 288(1–2):126–131. doi:10.1016/j.epsl.2009.09.014
- Kanamori H, Anderson DL (1975) Theoretical basis of some empirical relations in seismology. *Bull Seismol Soc Am* 65(5):1073–1095
- Kenner SJ, Segall P (2000) Postseismic deformation following the 1906 San Francisco earthquake. *J Geophys Res* 105(B6):13195–13209. doi:10.1029/2000JB900076
- Kenner SJ, Segall P (2003) Lower crustal structure in northern California: implications from strain rate variations following the 1906 San Francisco earthquake. *J Geophys Res* 108(B1):2011. doi:10.1029/2001JB000189
- Lachenbruch AH, Sass JH (1980) Heat-flow and energetics of the San Andreas fault zone. *J Geophys Res* 85(NB11):6185–6222. doi:10.1029/JB085iB11p06185
- Matthews MV, Segall P (1993) Estimation of depth-dependent fault slip from measured surface deformation with application to the 1906 San-Francisco earthquake. *J Geophys Res* 98(B7):12153–12163. doi:10.1029/93JB00440
- Pollitz FF, Nyst M (2005) A physical model for strain accumulation in the San Francisco Bay region. *Geophys J Int* 160(1):302–317. doi:10.1111/j.1365-246X.2005.02433.x
- Pollitz FF, Schwartz DP (2008) Probabilistic seismic hazard in the San Francisco Bay area based on a simplified viscoelastic cycle model of fault interactions. *J Geophys Res* 113(B5):B05409. doi:10.1029/2007JB005227
- Pollitz FF, Bakun WH, Nyst M (2004) A physical model for strain accumulation in the San Francisco Bay region: stress evolution since 1838. *J Geophys Res* 109(B11):B11408. doi:10.1029/2004JB003003
- Pollitz FF, McCrory P, Svarc J, Murray J (2008) Dislocation models of interseismic deformation in the western United States. *J Geophys Res* 113(B4):B04413. doi:10.1029/2007JB005174
- Prescott WH, Savage JC, Svarc JL, Manaker D (2001) Deformation across the Pacific-North America plate boundary near San Francisco, California. *J Geophys Res* 106(B4):6673–6682. doi:10.1029/2000JB900397
- Savage JC, Gan W, Prescott WH, Svarc JL (2004) Strain accumulation across the Coast Ranges at the latitude of San Francisco, 1994–2000. *J Geophys Res* 109(B3):B03413. doi:10.1029/2003JB002612
- Smith B, Sandwell D (2003) Coulomb stress accumulation along the San Andreas Fault system. *J. Geophys Res* 108(B6):2296. doi:10.1029/2002JB002136
- Thatcher W (1974) Strain release mechanism of 1906 San-Francisco earthquake. *Science* 184(4143):1283–1285. doi:10.1126/science.184.4143.1283
- Thatcher W (1975) Strain accumulation and release mechanism of 1906 San-Francisco earthquake. *J Geophys Res* 80(35):4862–4872. doi:10.1029/JB080i035p04862.
- Turcotte DL, Schubert G (2014) *Faulting*. In: *Geodynamics*. Cambridge University Press, New York, pp 361–364
- UNAVCO, Plate Boundary Observatory (PBO) (2012). <http://pbo.unavco.org/network>. Accessed 25 Aug 2012
- Yu TT, Rundle JB, Fernandez J (1996) Surface deformation due to a strike-slip fault in an elastic gravitational layer overlying a viscoelastic gravitational half-space. *J Geophys Res* 101(B2):3199–3214. doi:10.1029/95JB03118